Acta Crystallographica Section F
Structural Biology and Crystallization Communications
ISSN 1744-3091

Structures of BIR domains from human NAIP and cIAP2

Maria Dolores Herman,[a,b] Martin Moche,[c] Susanne Flodin,[c] Martin Welin,[c] Lionel Trésaugues,[c] Ida Johansson,[c] Martina Nilsson,[c] Pär Nordlund[a,c]* and Tomas Nyman[c]*

[a]Division of Biophysics, Department of Medical Biochemistry and Biophysics, Karolinska Institute, SE-17 177 Stockholm, Sweden, [b]Department of Biochemistry and Biophysics, Stockholm University, SE-106 91 Stockholm, Sweden, and [c]Structural Genomics Consortium, Karolinska Institute, SE-17 177 Stockholm, Sweden

Correspondence e-mail: par.nordlund@ki.se, tomas.nyman@ki.se

Received 4 June 2009
Accepted 23 September 2009

PDB References: NAIP BIR2, 2vm5, r2vm5sf; cIAP2 BIR3, 2uvl, r2uvlsf.

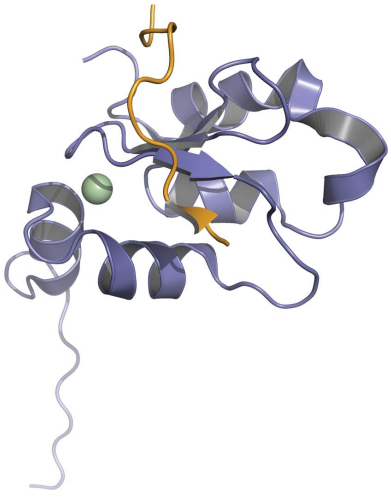

The inhibitor of apoptosis (IAP) family of proteins contains key modulators of apoptosis and inflammation that interact with caspases through baculovirus IAP-repeat (BIR) domains. Overexpression of IAP proteins frequently occurs in cancer cells, thus counteracting the activated apoptotic program. The IAP proteins have therefore emerged as promising targets for cancer therapy. In this work, X-ray crystallography was used to determine the first structures of BIR domains from human NAIP and cIAP2. Both structures harbour an N-terminal tetrapeptide in the conserved peptide-binding groove. The structures reveal that these two proteins bind the tetrapeptides in a similar mode as do other BIR domains. Detailed interactions are described for the P1′–P4′ side chains of the peptide, providing a structural basis for peptide-specific recognition. An arginine side chain in the P3′ position reveals favourable interactions with its hydrophobic moiety in the binding pocket, while hydrophobic residues in the P2′ and P4′ pockets make similar interactions to those seen in other BIR domain–peptide complexes. The structures also reveal how a serine in the P1′ position is accommodated in the binding pockets of NAIP and cIAP2. In addition to shedding light on the specificity determinants of these two proteins, the structures should now also provide a framework for future structure-based work targeting these proteins.

1. Introduction

The inhibitor of apoptosis (IAP) protein family plays a central role in apoptosis and inflammatory processes, conferring protection against cellular death. IAP proteins are modular and are characterized by the presence of one or more baculovirus IAP-repeats (BIR) domains. The BIR domain is a zinc-binding fold of approximately 70 residues that is essential for the anti-apoptotic properties of the IAPs. Eight members of the human IAP family have been identified and are equipped with either one BIR domain or a tandem repeat of three BIR domains (Salvesen & Duckett, 2002; Liston *et al.*, 2003). The most well studied member of the IAP family, X-linked IAP (XIAP), contains three BIR domains in tandem at the amino-terminus. XIAP binds and inhibits caspase 3 and 7 through the BIR2 domain and caspase 9 through the BIR3 domain (Deveraux *et al.*, 1999; Riedl *et al.*, 2001; Chai *et al.*, 2001; Shiozaki *et al.*, 2003; Scott *et al.*, 2005). These interactions are partly mediated by a surface groove on the BIR domain that binds amino-terminal tetrapeptides called IAP-binding motifs (IBMs). IBM sequences are displayed by caspase 3, 7 and 9 following proteolytic activation (Fuentes-Prior & Salvesen, 2004). The activity of IAPs is negatively regulated by several proteins, one of which is the secondary mitochondria-derived activator of caspases (Smac/DIABLO; Du *et al.*, 2000) that is released from the mitochondrial periplasmic space along with cytochrome *c* in response to apoptotic stimuli. After processing in the mitochondria, Smac/DIABLO displays an N-terminal IBM that binds XIAP and other IAPs, thereby interfering with the activity of these proteins (Verhagen *et al.*, 2000).

The closest paralogues to XIAP, cellular IAP 1 (cIAP1) and cellular IAP 2 (cIAP2), as well as neuronal apoptosis inhibitor protein (NAIP), contain three sequential BIR domains at their

N-terminus. cIAP1 and cIAP2 have been shown by several groups to ablate apoptosis when ectopically expressed in mammalian cells (Roy *et al.*, 1997; Simons *et al.*, 1999; Uren *et al.*, 1996). These and other studies indicated that these IAP proteins directly inhibit caspases (Davoodi *et al.*, 2004; Maier *et al.*, 2002; Roy *et al.*, 1997), but subsequent studies have suggested otherwise (Eckelman & Salvesen, 2006). Although they possess the conserved IBM-binding groove and have been reported to bind caspase 3, 7 and 9, these IAP proteins seem to lack the sequences necessary for inhibition of caspase activity (Eckelman *et al.*, 2006). It has been suggested that XIAP is the only bona fide caspase-inhibitory member of the IAP family (Eckelman *et al.*, 2006). The function of the other IAP-family members and the mechanism by which they repress caspase activity is not fully understood. In addition to their tandem of BIR domains, cIAP1 and cIAP2 contain an E3-ligase RING domain which could be involved in caspase ubiquitinylation, thus altering their substrate-interaction capability or labelling them for destruction (Huang *et al.*, 2000; Hao *et al.*, 2004; Vaux & Silke, 2005; Choi *et al.*, 2009). A role for cIAP1 and cIAP2 might also lie in the neutralization of IAP antagonists such as Smac/DIABLO, thus releasing the negative control of XIAP and allowing its inhibition of caspases (Wilkinson *et al.*, 2004; Eckelman & Salvesen, 2006). In addition to its three BIR domains, NAIP carries a nucleotide-oligomerization domain (NOD) followed by a C-terminal leucine-rich repeat (LRR). The presence of the NOD and LRR domains is unique among the IAPs and suggests that NAIP has functions that are distinct from those of the other IAP proteins. The LRR domain recognizes bacterially derived molecules in the cytosol. Hence, apart from anti-apoptotic activity mediated through the BIR domains, NAIP has been suggested to be involved in a caspase 1-mediated inflammation response through its NOD and LRR domains (Zamboni *et al.*, 2006).

Cancer cells evade apoptosis in part by overexpressing anti-apoptotic proteins and in some instances IAP-family proteins play a critical role in tumour maintenance and resistance to chemotherapy treatments (Hunter *et al.*, 2007; Vucic & Fairbrother, 2007). Therefore, IAP proteins represent potential targets for anticancer therapeutic treatment. To this end, peptides that bind selectively to the BIR domains of several IAP proteins and antagonize their interactions with caspases have been described (Fulda *et al.*, 2002; Yang *et al.*, 2003; Franklin *et al.*, 2003; Cossu *et al.*, 2009).

Given the central importance of BIR domains in the control of apoptosis and the potential therapeutic use of their inhibition, their functional and structural characterization is important. In this work, two new human BIR-domain structures are presented. The crystal structures of the cIAP2 BIR3 domain and the NAIP BIR2 domain represent the first BIR-domain structures for these proteins. In these structures, both BIR domains are stabilized by the N-terminus of the expression constructs that bind in the IBM groove. These structures show variations in peptide recognition compared with other structures and therefore provide new insights into the structural basis for peptide recognition in the IBM binding groove.

2. Materials and methods

2.1. Cloning and expression

Constructs encompassing residues 141–244 (BIR2 domain) and 244–337 (BIR3 domain) of human NAIP and cIAP2, respectively, were cloned into the pET-based vector pNIC-Bsa4a (Novagen) and expressed in *Escherichia coli* strain BL21 (DE3) (NAIP BIR2) and Rosetta 2 (DE3) (cIAP2 BIR3). Both recombinant proteins contained an N-terminal hexahistidine tag for purification and a TEV protease recognition site. Cell cultivation and protein expression were performed using the method described by Stenmark *et al.* (2007).

Table 1
Data collection, structure determination and refinement for NAIP BIR2 and cIAP2 BIR3.

Values in parentheses are for the outer shell.

	NAIP BIR2	cIAP2 BIR3
Data collection		
Beamline	BM14 (ESRF)	I911-3 (MAX-lab)
Wavelength (Å)	0.97627	0.97845
Space group	$P2_12_12_1$	$P2_12_12_1$
Unit-cell parameters (Å)		
a	36.5	49.4
b	43.1	53.7
c	57.0	85.6
Resolution limit (Å)	1.8 (1.85–1.80)	1.91 (1.96–1.91)
$I/\sigma(I)$	14.93 (3.86)	19.37 (3.93)
$R_{\rm merge}$† (%)	11.6 (59.1)	7.0 (59.7)
Completeness (%)	99.6 (99.3)	98.9 (97.3)
Redundancy	7.01 (7.13)	6.9 (7.3)
Refinement		
Resolution range (Å)	34.38–1.80	20.0–1.91
$R_{\rm work}$‡ (%)	17.8	20.2
$R_{\rm free}$‡ (%)	22.0	24.0
No. of reflections	8131	17150
Model		
No. of protein atoms	858	1557
No. of water molecules	51	103
No. of other atoms	6	6
B factors (Å^2)		
Proteins	17.3	29.7
Ligands	24.0	41.8
Water	35.0	56.3
Ramachandran plot§		
Residues in favoured regions (%)	97.0	96.8
Residues in allowed regions (%)	100	100
R.m.s. deviations		
Bond lengths (Å)	0.015	0.01
Bond angles (°)	1.324	1.07

† $R_{\rm merge} = \sum_{hkl}\sum_i |I_i(hkl) - \langle I(hkl)\rangle| / \sum_{hkl}\sum_i I_i(hkl)$, where $I_i(hkl)$ is the intensity measurement for a given reflection and $\langle I(hkl)\rangle$ is the average intensity for multiple measurements of this reflection. ‡ $R = \sum_{hkl} ||F_{\rm obs}| - |F_{\rm calc}|| / \sum_{hkl} |F_{\rm obs}|$, where $R_{\rm free}$ is calculated for a randomly chosen 5% of reflections which were not used for structure refinement and $R_{\rm work}$ is calculated for the remaining reflections. § The Ramachandran plot was calculated using *MolProbity* (Davis *et al.*, 2007).

2.2. Extraction and purification

The cell-extract preparation, purification protocol and buffer compositions were as described by Stenmark *et al.* (2007). NAIP BIR2 and cIAP2 BIR3 proteins were purified using an ÄKTAxpress system equipped with IMAC (HiTrap Chelating HP 1 ml, GE Healthcare) and gel-filtration (HiLoad 16/60 Superdex 75 prep grade, GE Healthcare) columns. Final gel filtration was performed at 277 K in 20 m*M* HEPES, 300 m*M* NaCl, 10% glycerol, 2 m*M* TCEP pH 7.5. The purity and integrity of the proteins were estimated by SDS–PAGE and electrospray MS (data not shown). NAIP BIR2 protein was concentrated to 24.5 mg ml^{-1} and cIAP2 BIR3 protein was concentrated to 16.2 mg ml^{-1}. The protein samples were frozen and stored in liquid nitrogen until further handling.

2.3. Crystallization and data collection

Crystals were obtained at room temperature by the hanging-drop vapour-diffusion method using 24-well plates (Hampton Research). For NAIP BIR2, 1 µl protein solution was mixed with 1 µl well solution consisting of 0.1 *M* citric acid pH 5.0 and 20% PEG 6000. For cIAP2 BIR3, 1 µl protein solution was mixed with 1 µl well solution consisting of 16% PEG 8000, 40 m*M* potassium phosphate and 20%

glycerol. NAIP BIR2 crystals were briefly soaked in a cryoprotectant solution composed of the reservoir solution supplemented with 20%(*v*/*v*) glycerol and frozen in liquid nitrogen. cIAP2 BIR3 crystals were directly frozen after being harvested from the drop. X-ray data were collected at 100 K on beamlines BM14 at the European Synchrotron Radiation Facility (ESRF) and I911-3 at MAX-lab for NAIP BIR2 and cIAP2 BIR3, respectively.

2.4. Phasing, model building and refinement

Data sets were processed and scaled with *XDS* and *XSCALE* (Kabsch, 1993). Both structures were solved by molecular replacement using *MOLREP* (Vagin & Teplyakov, 1997). As search models, the PDB structures 1oxn and 2uvl were used for cIAP2 and NAIP, respectively. The initial model was then automatically built using *ARP*/*WARP* (Perrakis *et al.*, 1999). Final models were obtained after iterative cycles of manual model building in *Coot* (Emsley & Cowtan, 2004) and maximum-likelihood refinement in *REFMAC*5 (Murshudov *et al.*, 1997). Space groups, unit-cell parameters and statistics are listed in Table 1. Coordinates and structure factors for NAIP BIR2 and cIAP2 BIR3 have been deposited in the Protein Data Bank (PDB) with accession codes 2vm5 and 2uvl, respectively. Structure analysis was performed using *Coot* and *PyMOL* (DeLano Scientific, Palo Alto, California, USA). Figures were produced using *PyMOL*.

3. Results

3.1. Overall structure

The NAIP BIR2 and cIAP2 BIR3 structures display the conserved BIR-domain fold, with two or three N-terminal α-helices, a central three-stranded antiparallel β-sheet and two or three C-terminal α-helices (Fig. 1). The IBM binding groove is formed between the last

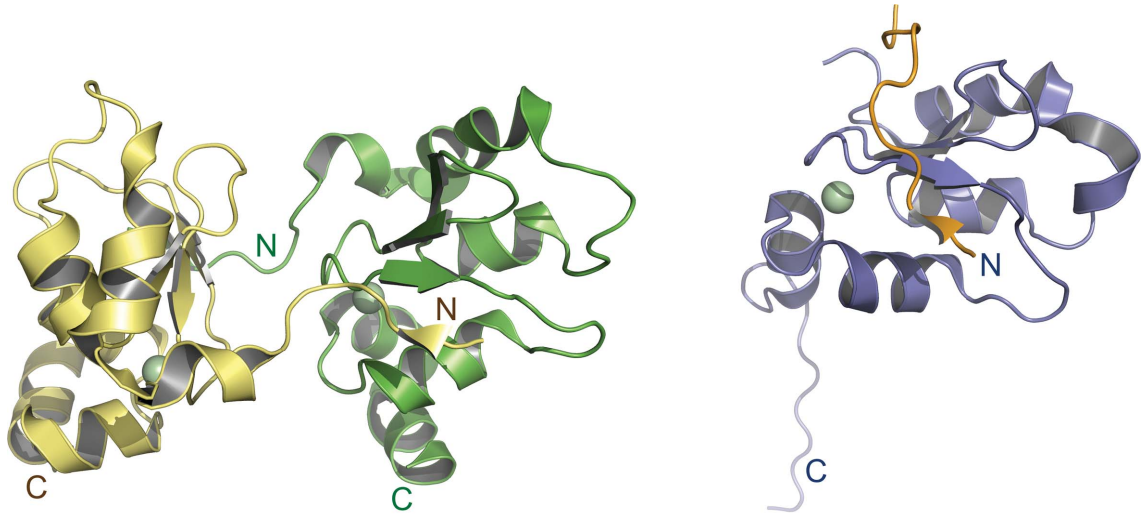

Figure 1
(*a*) Schematic representation of the structure of the cIAP2 BIR3 domain. An experimentally achieved dimer constitutes the asymmetric unit. The N-termini bind in the peptide-binding pockets of the BIR domains, forming an extension of the central β-sheet. (*b*) Schematic representation of the NAIP BIR2-domain structure. The N-terminus, shown in yellow, binds in the peptide-binding pocket similarly as in the cIAP2 BIR3 structure.

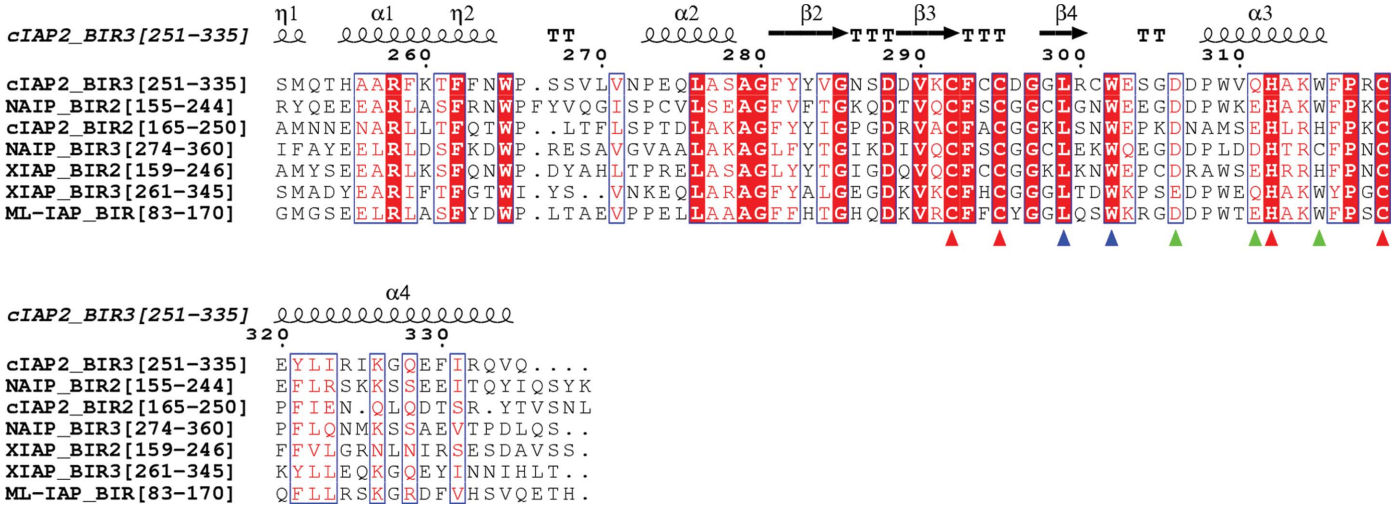

Figure 2
Sequence alignment of BIR domains. The sequences of the described BIR3 and BIR2 domains from human cIAP2 and NAIP are compared with the corresponding BIR domains from XIAP. The ML-IAP BIR domain structure was used as search model for molecular replacement. Colour markers: red triangles, Zn^{2+}-chelating residues; green triangles, residues of high importance for IBM interaction (see text for details); blue triangles, conserved residues lining a hydrophobic cavity at the P1′ binding position.

strand of the central β-sheet and the following α-helix. As in other BIR domains, a Zn^{2+} ion is chelated by one histidine and three cysteine residues. The chelating residues are strictly conserved in all BIR domains and are contributed by the central β-sheet part and the C-terminal α-helices (Fig. 2). As the Zn^{2+} ion is completely buried in the fold, it is most likely to have a strictly structural function.

The cIAP2 BIR3 domain crystallized with two molecules in the asymmetric unit. The first four residues of the proteolytically generated N-terminus of monomer *A* make an intermolecular interaction with the IBM-binding groove of monomer *B* and *vice versa* (Fig. 1*a*). The N-terminus of the cIAP2 BIR3 polypeptide precedes the BIR domain by eight residues. The N-terminus of the NAIP BIR2 domain is also bound to the IBM-binding groove, but in this case intramolecularly, and the asymmetric unit only contains one molecule (Fig. 1*b*). The N-terminus of the NAIP BIR2 domain-containing polypeptide precedes the first helix of the BIR fold by 18 residues. In the present NAIP BIR2 structure the sequence corresponding to the C-terminal helix of other known BIR-domain structures appears as random coil. This conformation is apparently stabilized by crystal packing, as the sequence makes contact with three neighbouring BIR molecules.

3.2. Interactions in the peptide-binding groove

In the following discussion of different tetrapeptides binding in the IBM-binding groove, the IBM residues are denoted P1′–P4′ according to their position in the sequence. Fig. 3(*a*) shows a superposition of the cIAP2 BIR3 and NAIP BIR2 structures. cIAP2 binds the N-terminal sequence SMRY in the IBM-binding groove, coordinated by the conserved residues Asp306, Gln311 and Trp315 (Fig. 2). NAIP BIR2 binds the N-terminal tetrapeptide SMRV in the IBM groove, coordinated by the corresponding residues Asp211, Glu216 and Trp220.

Asp306 of cIAP2 and the corresponding Asp211 of NAIP coordinate the N-terminal amino group *via* a salt bridge (Fig. 3*a*). This interaction explains why the tetrapeptides that bind to the IBM-binding grooves are preferably N-terminal. The residue at this position is highly conserved as an Asp or Glu in human BIR domains and the D214S mutation in the corresponding position of XIAP BIR2 has been shown to abolish or significantly reduce interaction with IAP-binding proteins (Verhagen *et al.*, 2007).

In both structures the N-terminal serine is bound to the P1′ binding position of the IBM-binding groove. In most reported structures of BIR–peptide complexes the first residue of the peptide is Ala. The β-methyl group of this Ala is then buried in a small hydrophobic pocket formed by strictly conserved Leu and Trp residues (Leu299 and Trp302 in cIAP2; Fig. 2). In both of the structures reported here the Ser side chain is now buried in this pocket (Fig. 3*b*). Residues Gln311 of cIAP2 BIR3 and the corresponding Glu216 of NAIP BIR2 form hydrogen bonds to the O^{γ} atom of the P1′ serine side chain. These positions are invariably occupied by a Glu or a Gln residue in BIR domains (Fig. 2). The backbone O atom of the P1′ residue interacts with the N^{ε} atom of the Trp315/Trp220 side chain, forming a hydrogen bond. This position in the IBM-binding groove is occupied by a Trp or a His residue in most BIR domains. The His at this position then forms an equivalent hydrogen bond through its N^{ε} atom to the P1′ residue O atom.

The Trp315/Trp220 side chains make hydrophobic interactions with the aliphatic side-chain C atoms of the Arg at the P3′ position of the tetrapeptide. This provides an explanation for the results of a recent

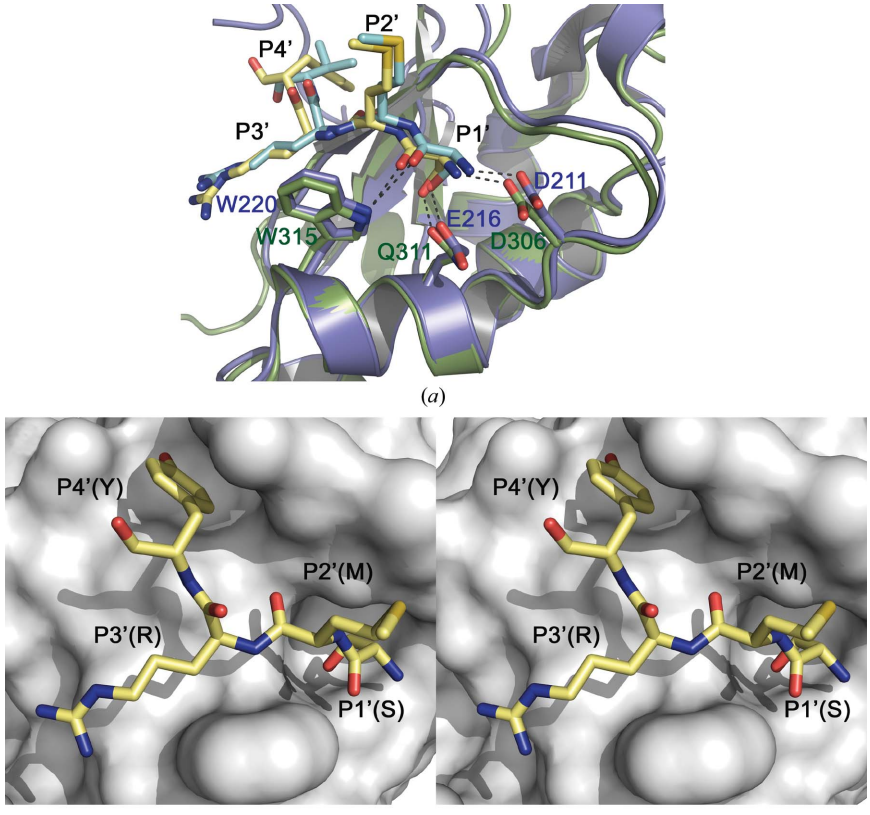

Figure 3
Representation of the IBM-binding site of the BIR domains. (*a*) Superposition of cIAP2 BIR3 (green/yellow) with NAIP BIR2 (blue/light blue). (*b*) Stereo diagram showing the IBM-binding pocket of cIAP2 BIR3 with the N-terminal peptide SMRY in yellow.

random peptide library study, in which a propensity for binding Arg at this position was suggested for the NAIP BIR2 domain (Eckelman *et al.*, 2008). A proline often occupies the P3′ position of IBMs. Its side chain also contributes to the stability of the complex by hydrophobic interaction with the pocket-lining Trp, corresponding to Trp315/Trp220 in the present structures, and the following residue, which is conserved as a Phe/Tyr. The presence of a Tyr in cIAP2 and a Val in NAIP at the P4′ residue position are consistent with the previously suggested strong preference for hydrophobic residues with branched C^{β} atoms at this position (Franklin *et al.*, 2003; Eckelman *et al.*, 2008).

Overall, backbone interactions of the tetrapeptide with the IBM-binding groove provide the basis of the stability of BIR domain–IBM complexes. The tetrapeptide forms an extension of the antiparallel β-sheet of the BIR-domain fold, providing it with a fourth strand stabilized by the backbone N and O atoms of the P2′ residue and the N atom of the P4′ residue.

3.3. Comparison of the cIAP2 BIR3 and NAIP BIR2 domains with the BIR3 and BIR2 domains of XIAP

Fig. 4(*a*) shows a superposition of the cIAP2 BIR3 structure with the XIAP BIR3 structure in complex with the caspase 9 small subunit N-terminal tetrapeptide ATPF (Shiozaki *et al.*, 2003). The backbone of the IBM peptides overlaps with an r.m.s.d. of 1.27 Å (0.87 Å for P1′–P3′). The strong contribution of backbone interactions to the binding of N-terminal tetrapeptides and the conservation of key residues interacting with the IBM side chains suggests that BIR domains display an overlapping specificity for caspase IBM motifs. However, the binding of BIR domains to caspases alone is not sufficient for caspase inhibition. Rather, the inhibiting elements of XIAP lie in the linker region preceding the BIR2 domain, part of which binds and blocks the catalytic site of caspase 3 and 7, and in the last helix of the BIR3 domain, which inhibits caspase 9 dimer formation (Riedl *et al.*, 2001; Chai *et al.*, 2001; Shiozaki *et al.*, 2003).

Comparison of the NAIP BIR2 structure with XIAP BIR2 in complex with caspase 3 (Riedl *et al.*, 2001; Fig. 4*b*) is interesting, as the BIR2 domains of NAIP, cIAP1, cIAP2 and XIAP have all been reported to bind caspase 3 and 7 (Riedl *et al.*, 2001; Chai *et al.*, 2001; Shiozaki *et al.*, 2003; Maier *et al.*, 2002; Eckelman & Salvesen, 2006; Eckelman *et al.*, 2006) and the processed forms of the small subunit of the active caspase 3 and 7 dimer start with a serine (Fuentes-Prior & Salvesen, 2004). The two IBM tetrapeptides overlap with an r.m.s.d. of 0.68 Å (0.55 Å for P1′–P3′). The P1′ Ser side chain is buried in the corresponding pocket and the O^{γ} atom forms a hydrogen bond to the Asp side chain at positions Asp211 (cIAP2) and Asp214 (XIAP).

4. Discussion

This work describes the crystal structures of the BIR2 domain of human NAIP and the BIR3 domain of human cIAP2. Both structures are stabilized by binding of the amino-terminus in their peptide-interaction groove. Although the N-termini are generated serendipitously, their sequences have similar properties to the well characterized physiological interaction peptides for BIR domains. This suggests that these structures may provide information about the binding specificity of these BIR domains.

A number of tetrapeptides have been found to bind to the IBM groove of different BIR domains, although with different affinities. The reason for this apparent promiscuity partly lies in the fact that the main part of the interaction is provided by the tetrapeptide backbone, resulting in the formation of an additional strand to the β-sheet of the BIR domain. It can now be concluded that the same interaction mode is seen in the present structures.

As discussed above, the P1′ residue side chain binds in a small hydrophobic pocket formed by the conserved Leu and Trp in the L*XX*W motif (Fig. 2). In studies performed on peptide preferences, Ala is by far (>98%) the most preferred residue at the P1′ position (Franklin *et al.*, 2003; Eckelman *et al.*, 2008). Interestingly, Ser, which is present in the peptides binding in the IBM pockets in this work, is among the few other (weakly) preferred residues at this position. Notably, glycine does not display even a weak occurrence at this position, indicating a significant contribution of the P1′ Ala or Ser side chain to the IBM-binding affinity.

Although serine displays a relatively low preference in the P1′ binding site, it is interesting to note that proteolytically generated forms of the caspase 3 and 7 small subunits can display a serine as an altervative to alanine as the N-terminal residue. These caspases have been shown to bind to several IAP-family members, including NAIP and cIAP2 (Maier *et al.*, 2002). It is likely that the different caspase N-termini have different affinities for different BIR domains and this may render the caspases less or more receptive to BIR-mediated

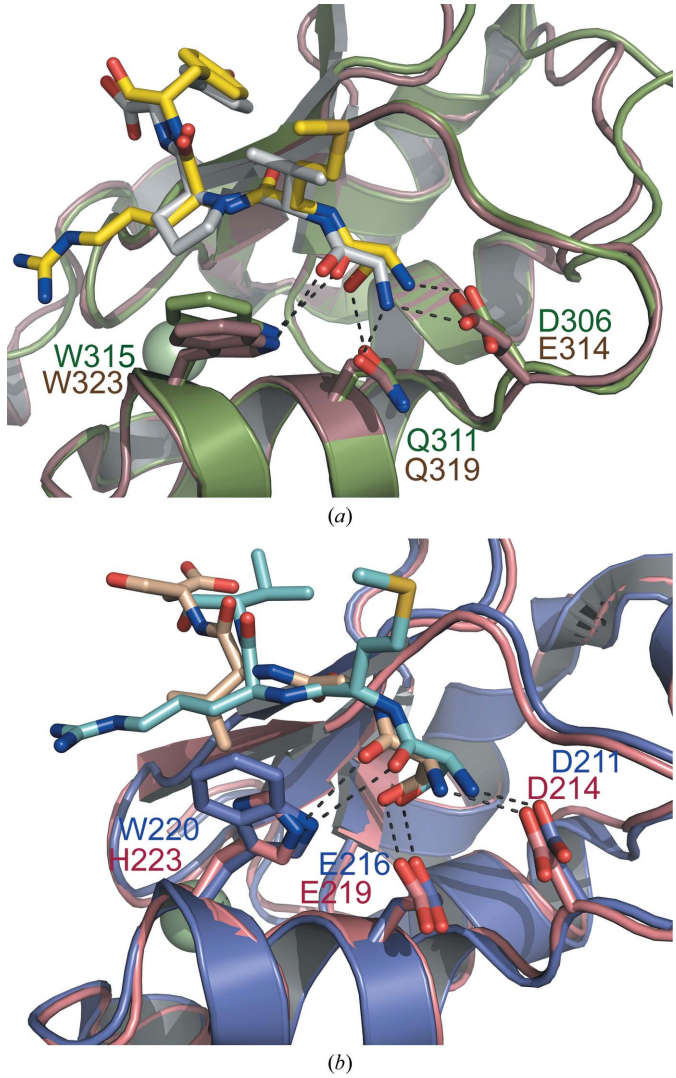

Figure 4
Comparison of interactions in the IBM-binding cleft. (*a*) Superposition of cIAP2 BIR3 (green/yellow) with XIAP BIR3 (brown/white). (*b*) Superposition of NAIP BIR2 (blue/light blue) with XIAP BIR2 (pink) bound to the N-terminus of the processed caspase-3 small domain (sand).

regulation. Moreover, in a recent study mitochondrial glutamate dehydrogenase, which carries a Ser as the first residue after N-terminal processing, has been identified as an IAP-interacting protein (Verhagen *et al.*, 2007).

The particular side chains at positions P2′–P4′ confer additional stability on the interaction. Mainly hydrophobic interactions are preferred at these binding sites. Previous studies have shown that a proline is by far the most preferred residue at the P3′ position (Franklin *et al.*, 2003; Eckelman *et al.*, 2008). Exceptions to this are displayed by the BIR2 domains of XIAP, cIAP1 and NAIP. In the XIAP BIR2 domain Ala seems to be the preferred residue, in cIAP1 BIR2 Lys and Arg are prominent and in NAIP BIR2 Arg and Pro seem to have equal preference. In the structures presented here, Arg is found at the P3′ position, stabilized by interaction with the Trp lining the IBM-binding groove of both structures. This confirms the recently made suggestion that an Arg can be preferred at this position, particularly in the case of NAIP BIR2 (Eckelman *et al.*, 2008).

Although the caspase-inhibiting activities of IAPs other than XIAP have been questioned (Eckelman *et al.*, 2006), there is little doubt that NAIP, cIAP1 and cIAP2 indeed bind to and affect the activities of caspases. Furthermore, their overexpression protects the cell from apoptotic stimuli. In this work, we present the first crystal structures of BIR domains from human NAIP and cIAP2. These structures confirm that the peptide-interaction modes are similar to those seen in other BIR domains. These structures also reveal a favourable interaction of the hydrophobic moiety of the Arg side chain at the P3′ position and explain why Ser can be accepted at the P1 position in these proteins. Together, these structures therefore contribute novel structural information on BIR–peptide interactions and should also provide a framework for structure-based drug design in the future.

The authors wish to thank the staff at beamline BM14 at the ESRF Grenoble and at beamline I911-3 at MAX-lab, Lund for technical assistance. The Structural Genomics Consortium is a registered charity (No. 1097737) that receives funds from the Canadian Institutes for Health Research, the Canadian Foundation for Innovation, Genome Canada through the Ontario Genomics Institute, GlaxoSmithKline, Karolinska Institutet, the Knut and Alice Wallenberg Foundation, the Ontario Innovation Trust, the Ontario Ministry for Research and Innovation, Merck & Co. Inc., the Novartis Research Foundation, the Swedish Agency for Innovation Systems, the Swedish Foundation for Strategic Research and the Wellcome Trust. The work was also supported by EU SPINE II, the Swedish Cancer Society and the Swedish Research Council (PN).

References

Chai, J., Shiozaki, E., Srinivasula, S. M., Wu, Q., Datta, P., Alnemri, E. S. & Shi, Y. (2001). *Cell*, **104**, 769–780.
Choi, Y. E., Butterworth, M., Malladi, S., Duckett, C. S., Cohen, G. M. & Bratton, S. B. (2009). *J. Biol. Chem.* **284**, 12772–12782.
Cossu, F., Mastrangelo, E., Milani, M., Sorrentino, G., Lecis, D., Delia, D., Manzoni, L., Seneci, P., Scolastico, C. & Bolognesi, M. (2009). *Biochem. Biophys. Res. Commun.* **378**, 162–167.
Davis, I. W., Leaver-Fay, A., Chen, V. B., Block, J. N., Kapral, G. J., Wang, X., Murray, L. W., Arendall, W. B. III, Snoeyink, J., Richardson, J. S. & Richardson, D. C. (2007). *Nucleic Acids Res.* **35**, W375–W383.
Davoodi, J., Lin, L., Kelly, J., Liston, P. & MacKenzie, A. E. (2004). *J. Biol. Chem.* **279**, 40622–40628.
Deveraux, Q. L., Leo, E., Stennicke, H. R., Welsh, K., Salvesen, G. S. & Reed, J. C. (1999). *EMBO J.* **18**, 5242–5251.
Du, C., Fang, M., Li, Y., Li, L. & Wang, X. (2000). *Cell*, **102**, 33–42.
Eckelman, B. P., Drag, M., Snipas, S. J. & Salvesen, G. S. (2008). *Cell Death Differ.* **15**, 920–928.
Eckelman, B. P. & Salvesen, G. S. (2006). *J. Biol. Chem.* **281**, 3254–3260.
Eckelman, B. P., Salvesen, G. S. & Scott, F. L. (2006). *EMBO Rep.* **7**, 988–994.
Emsley, P. & Cowtan, K. (2004). *Acta Cryst.* D**60**, 2126–2132.
Franklin, M. C., Kadkhodayan, S., Ackerly, H., Alexandru, D., Distefano, M. D., Elliott, L. O., Flygare, J. A., Mausisa, G., Okawa, D. C., Ong, D., Vucic, D., Deshayes, K. & Fairbrother, W. J. (2003). *Biochemistry*, **42**, 8223–8231.
Fuentes-Prior, P. & Salvesen, G. S. (2004). *Biochem. J.* **384**, 201–232.
Fulda, S., Wick, W., Weller, M. & Debatin, K. M. (2002). *Nature Med.* **8**, 808–815.
Hao, Y., Sekine, K., Kawabata, A., Nakamura, H., Ishioka, T., Ohata, H., Katayama, R., Hashimoto, C., Zhang, X., Noda, T., Tsuruo, T. & Naito, M. (2004). *Nature Cell Biol.* **6**, 849–860.
Huang, H., Joazeiro, C. A., Bonfoco, E., Kamada, S., Leverson, J. D. & Hunter, T. (2000). *J. Biol. Chem.* **275**, 26661–26664.
Hunter, A. M., LaCasse, E. C. & Korneluk, R. G. (2007). *Apoptosis*, **12**, 1543–1568.
Kabsch, W. (1993). *J. Appl. Cryst.* **26**, 795–800.
Liston, P., Fong, W. G. & Korneluk, R. G. (2003). *Oncogene*, **22**, 8568–8580.
Maier, J. K., Lahoua, Z., Gendron, N. H., Fetni, R., Johnston, A., Davoodi, J., Rasper, D., Roy, S., Slack, R. S., Nicholson, D. W. & MacKenzie, A. E. (2002). *J. Neurosci.* **22**, 2035–2043.
Murshudov, G. N., Vagin, A. A. & Dodson, E. J. (1997). *Acta Cryst.* D**53**, 240–255.
Perrakis, A., Morris, R. & Lamzin, V. S. (1999). *Nature Struct. Biol.* **6**, 458–463.
Riedl, S. J., Renatus, M., Schwarzenbacher, R., Zhou, Q., Sun, C., Fesik, S. W., Liddington, R. C. & Salvesen, G. S. (2001). *Cell*, **104**, 791–800.
Roy, N., Deveraux, Q. L., Takahashi, R., Salvesen, G. S. & Reed, J. C. (1997). *EMBO J.* **16**, 6914–6925.
Salvesen, G. S. & Duckett, C. S. (2002). *Nature Rev. Mol. Cell Biol.* **3**, 401–410.
Scott, F. L., Denault, J. B., Riedl, S. J., Shin, H., Renatus, M. & Salvesen, G. S. (2005). *EMBO J.* **24**, 645–655.
Shiozaki, E. N., Chai, J., Rigotti, D. J., Riedl, S. J., Li, P., Srinivasula, S. M., Alnemri, E. S., Fairman, R. & Shi, Y. (2003). *Mol. Cell*, **11**, 519–527.
Simons, M., Beinroth, S., Gleichmann, M., Liston, P., Korneluk, R. G., MacKenzie, A. E., Bahr, M., Klockgether, T., Robertson, G. S., Weller, M. & Schulz, J. B. (1999). *J. Neurochem.* **72**, 292–301.
Stenmark, P., Ogg, D., Flodin, S., Flores, A., Kotenyova, T., Nyman, T., Nordlund, P. & Kursula, P. (2007). *J. Neurochem.* **101**, 906–917.
Uren, A. G., Pakusch, M., Hawkins, C. J., Puls, K. L. & Vaux, D. L. (1996). *Proc. Natl Acad. Sci. USA*, **93**, 4974–4978.
Vagin, A. & Teplyakov, A. (1997). *J. Appl. Cryst.* **30**, 1022–1025.
Vaux, D. L. & Silke, J. (2005). *Nature Rev. Mol. Cell Biol.* **6**, 287–297.
Verhagen, A. M., Ekert, P. G., Pakusch, M., Silke, J., Connolly, L. M., Reid, G. E., Moritz, R. L., Simpson, R. J. & Vaux, D. L. (2000). *Cell*, **102**, 43–53.
Verhagen, A. M., Kratina, T. K., Hawkins, C. J., Silke, J., Ekert, P. G. & Vaux, D. L. (2007). *Cell Death Differ.* **14**, 348–357.
Vucic, D. & Fairbrother, W. J. (2007). *Clin. Cancer Res.* **13**, 5995–6000.
Wilkinson, J. C., Wilkinson, A. S., Scott, F. L., Csomos, R. A., Salvesen, G. S. & Duckett, C. S. (2004). *J. Biol. Chem.* **279**, 51082–51090.
Yang, L., Mashima, T., Sato, S., Mochizuki, M., Sakamoto, H., Yamori, T., Oh-Hara, T. & Tsuruo, T. (2003). *Cancer Res.* **63**, 831–837.
Zamboni, D. S., Kobayashi, K. S., Kohlsdorf, T., Ogura, Y., Long, E. M., Vance, R. E., Kuida, K., Mariathasan, S., Dixit, V. M., Flavell, R. A., Dietrich, W. F. & Roy, C. R. (2006). *Nature Immunol.* **7**, 318–325.